Journal of Molecular Liquids 391 (2023) 123069

Contents lists available at ScienceDirect

Journal of Molecular Liquids

journal homepage: www.elsevier.com/locate/molliq

The relaxation dynamics and dielectric properties of cyanobiphenyl-based nematic tripod liquid crystals

Jordan Hobbs [a], Matthew Reynolds [a], Mallasandra Krishnappa Srinatha [b,c], Govindaswamy Shanker [c], Johan Mattsson [a,*], Mamatha Nagaraj [a,*]

[a] School of Physics and Astronomy, University of Leeds, LS2 9BW, United Kingdom
[b] Present address: Department of Chemical Science, Institute of Science Education and Research, Mohali-140306, India
[c] Department of Chemistry, Bangalore University, Jnana Bharathi Campus, Bengaluru, 560056, India

ARTICLE INFO

Dataset link: https://doi.org/10.5518/1405

Keywords:
Liquid crystals
Tripods
Glass formation
Dynamics
Dielectric properties

ABSTRACT

We present a detailed investigation of the phase behaviour, molecular relaxation dynamics, rheology and dielectric properties of two cyanobiphenyl-based liquid crystal (LC) tripods, differing only in the length of their spacer units (6 or 9 carbons). These LC tripods combine properties of low molecular weight LCs and LC polymers, resulting in a range of advantageous properties including a wide nematic range ($\Delta T > 90$ K) and a large birefringence (0.3 at $T - T_{NI} = -80$ K for the 6 spacer tripod). Using broadband dielectric relaxation spectroscopy, calorimetry, oscillatory and steady state shear rheology, we identified four molecular relaxation processes: the structural (α) relaxation (defining the glass transition temperature, T_g); the δ relaxation (reorientation of the mesogen unit around its short axis); the β relaxation (reorientation around its long axis); and the γ relaxation (internal tripod arm fluctuations). The β and γ relaxations follow Arrhenius temperature dependencies in the glass, whereas the α and δ relaxations merge above, but near T_g, where they follow a non-Arrhenius VFT behaviour. For higher temperatures, the two relaxations separate and for $T > T^*$, where T^* marks a dynamic crossover, the α relaxation transitions from VFT to Arrhenius behaviour. For the two tripods, ratios of $T^*/T_g = 1.14$ and $T^*/T_g = 1.13$ were observed respectively, consistent with the ratio observed for many side-chain LC polymers (and other LC systems), and consistent with the ratio where a dynamic crossover is typically observed also for non-LC glass-formers. However, for non-LC systems, the transition to Arrhenius behaviour happens at significantly higher temperatures relative to T_g and the dynamic crossover at T^* is typically observed as a transition between two different VFT behaviours. We argue that for the tripods these differences arise from differences in the molecular relaxation mechanisms induced by the LC order. Finally, for temperatures where δ and α relaxations are separated, we find that ion conductivity decouples from the α relaxation, instead following the δ relaxation; this demonstrates that the ion transport properties for the tripods can be tuned by the design of the tripod mesogen arm.

1. Introduction

Liquid crystals (LCs) are important for a wide range of applications including liquid crystal displays [1], and photonic or electronic devices [2], such as photonic fibres [3] or beam steering devices [4]. Many of these applications involve low molecular weight calamitic LCs which are characterised by low viscosities and correspondingly fast phase switching times. Alternatively, LC polymers (LCPs) have been synthesized both as main chain LCPs, where the mesogenic moieties are present in the polymer backbone, and as side-chain LCPs (SCLCPs) where the mesogenic moiety is separated from the backbone by a flexible spacer [5]. Polymers have advantages in terms of the increased tuneability of material properties provided by the chain-length and flexibility. However, LCPs are typically highly viscous, leading to slow phase switching and the desired LC phases often forming at relatively high temperatures [6], rendering realistic applications difficult. Oligomeric LCs, on the other hand, can combine many of the beneficial properties of LC polymers with the lower viscosity typically found in low molecular weight LCs, thus allowing lower transition temperatures and faster phase switching times.

* Corresponding authors.
E-mail addresses: k.j.l.mattsson@leeds.ac.uk (J. Mattsson), M.Nagaraj@leeds.ac.uk (M. Nagaraj).

https://doi.org/10.1016/j.molliq.2023.123069
Received 15 April 2023; Received in revised form 21 August 2023; Accepted 13 September 2023
Available online 21 September 2023

Many studies of oligomeric LCs have focused on dimers [7–11], consisting of two mesogenic groups separated by a flexible spacer, due to the prevalence of novel phase structures such as the twist-bend nematic phase [12] and the twist-bend smectic C phase [13]. Also trimers have been investigated even though the studies, so far, have mainly focused on interesting phase behaviour, including the formation of intercalated smectic phases [14], and the possible existence of a biaxial phase [15]. Trimeric LCs of varying geometries have also been investigated, e.g. including linear structures where the mesogenic units are separated by flexible spacers [14,16–18], or branched tripod molecules where the mesogenic units are appended to a central core [14,19–25]. Tripod LCs [24,25], the focus of the present work, are relatively new materials and are interesting as low melting point materials, characterised by a wide nematic range, and thus with potential use in room temperature LC-applications.

When a molecular liquid or polymer melt is cooled, the structural (α) relaxation slows down, and if crystallization is avoided (e.g. by fast cooling), this will eventually lead to the liquid or melt falling out of equilibrium, resulting in a disordered solid - a glass. Correspondingly, LC polymers also form glassy states at low temperatures [26–32], and non-polymeric molecular LCs, both single component [33–37] and mixtures [38], form glasses even though specific sample preparation methods are often needed to prevent crystallization. Importantly, for LC liquids or polymers, the anisotropy present in the LC phase at vitrification is retained, which means that LC-based glasses are solids characterised by molecular anisotropy.

The glass transition temperature T_g is commonly defined as the temperature for which the characteristic relaxation time of the α relaxation $\tau_\alpha = 100$ s [39]. In addition to the structural α relaxation, non-LC glass-forming liquids or polymers typically show additional 'secondary' relaxations that correspond to more local molecular motions; these are normally termed β, γ, δ ... in order of decreasing characteristic relaxation time for a fixed temperature. At least one of these, the β relaxation (sometimes called the Johari-Goldstein β relaxation [40]), is believed to be generic to glass-formation and has been shown to have strong links to the structural α relaxation [39,41–43].

In the glassy state, where the structure is largely frozen, the characteristic relaxation time τ for a particular relaxation typically follows Arrhenius behaviour,

$$\tau = \tau_0 \exp\left[\frac{\Delta H}{RT}\right], \tag{1}$$

where τ_0 is a microscopic relaxation time ($\sim 10^{-13}$ s), ΔH is the activation enthalpy, R is the gas constant and T the temperature. In contrast - the temperature (T) dependence of the α relaxation is often described well using a so-called Vogel Fulcher Tammann (VFT) equation for temperatures near but above T_g [32,43],

$$\tau_\alpha(T) = \tau_0 \exp\left[\frac{DT_0}{T - T_0}\right], \tag{2}$$

where τ_0 is a microscopic relaxation time ($\sim 10^{-13}$ s), D controls the T-sensitivity, the so-called fragility [44], and T_0 is a temperature for which τ would diverge if the equilibrium VFT-behaviour persisted to low-T. The fragility, i.e. the sensitivity to a T-change near T_g, is alternatively often defined more directly as the slope of $\tau_\alpha(T)$ at T_g in an Arrhenius plot m [45]:

$$m = \left.\frac{d \log \tau_\alpha}{d(T_g/T)}\right|_{T=T_g}. \tag{3}$$

Thus, 'fragile' liquids are sensitive to a T-change near T_g and are thus characterised by a large m, or conversely a small D, whereas 'strong' liquids are insensitive to a T-change, and are thus characterised by more Arrhenius-like behaviour.

The VFT expression often provides a good empirical description of $\tau_\alpha(T)$ over an extended T-range for $T \leq T_g$. However, for T above a crossover temperature T_B the $\tau_\alpha(T)$ behaviour for non-LC glass-forming liquids typically crosses over into another VFT-like $\tau_\alpha(T)$ dependence, normally more markedly non-Arrhenius (more fragile) [46]. The cross-over temperature T_B generally has values $T_B/T_g \sim 1.2 - 1.6$, and a correlation between the T_B/T_g ratio and fragility has been proposed [47]. The dynamic crossover at T_B is also typically manifested in other changes in the liquid behaviour, including the separation of the α and β relaxations [48,49], a decoupling between translational and rotational diffusion [43], and changes in the T-dependence of the α-relaxation strength [50]. Thus, T_B corresponds to a fundamental change in the liquid dynamics and such behaviour was predicted in 1969 by Goldstein [51] and associated with the relevant energy barriers becoming significantly larger than thermal energy for $T < T_B$. For T larger than a temperature T_A ($T_A > T_B > T_g$), on the other hand, the α relaxation can take place without need for significant cooperative motion and an Arrhenius behaviour describes the data well [46].

Oligomers and polymers generally display glass-transition dynamics with similar characteristics to those in non-polymeric glass-formers. However, the chain connectivity and presence of intramolecular degrees of freedom leads to a more complicated inter-relationship between the structural α and secondary relaxations [52,53]. Also, for chains longer than one or a few Rouse beads, the change in $\tau_\alpha(T)$ at $T \approx T_B$ often disappears, and one effective VFT behaviour can fit the data over a very wide T-range [54,55]. Moreover, the change at T_A is often difficult to observe for polymers due to sample degradation before these relatively high temperatures are reached [56].

The general theory for the dielectric relaxation of rigid dipolar molecules in nematic fluids was developed by Nordio et al. [57]. Four molecular relaxation modes are generally observed which include both rotation around the mesogen long axis, and three different rotations around the corresponding short axis [58]. Neglecting molecular biaxiality, the relaxation strengths of the different processes are written in terms of dipole components using the Maier and Meir equations [59,60].

As discussed in detail below, the relaxation dynamics of the tripod LCs investigated in this work show significant similarities to the dynamics of SCLCPs rather than low molecular weight nematic LCs. SCLCPs have been relatively thoroughly studied. The key elements of their dynamics are outlined in the following: The structural α relaxation of SCLCPs, directly related to glass-formation, is generally associated with the segmental motions of the backbone [61,62]. Importantly, as for non-LC glass-formers, $\tau_\alpha(T)$ generally demonstrates a cross-over in dynamics at a crossover temperature $T^\star \sim 1.1 - 1.3 \times T_g$ [26,30,31,63–67]. Thus, $T^\star/T_g$ is similar to T_B/T_g for non-LC glass-formers, suggesting that they have similar origin. However, in contrast to the behaviour for non-LC glass-formers, SCLCPs typically show a transition from a low-T VFT to a high-T Arrhenius behaviour, and it appears that this transition to Arrhenius behaviour is directly linked to the formation of LC phases [64]. The same conclusion was also reached for a LC elastomer which could be produced either in a nematic or an isotropic phase, where the low-T Arrhenius behaviour was associated with the presence of nematic fluctuations [68].

For SCLCPs, in addition to the α relaxation, a slower so-called δ relaxation, and up to three faster β, γ_1, and γ_2 relaxations, are often observed. The δ relaxation is generally interpreted as due to rotations of the mesogenic unit around its short axis [26–28]; this rearrangement requires the mobility of the α relaxation and the δ relaxation is thus generally slower than the α relaxation. The β relaxation for SCLCPs (not to be confused with the β relaxation in non-LC glass-formers, as discussed above), in turn, is typically attributed to the rotation of the mesogenic unit around its long axis [30,61,69], and its corresponding activation energy strongly depends on the structure of the mesophase frozen into the glass [70–72]. Finally, the γ_1 and γ_2 relaxations are typically assigned to fluctuations of the tail and spacer groups, respectively; the activation energies for these relaxations are normally relatively independent of spacer length [70].

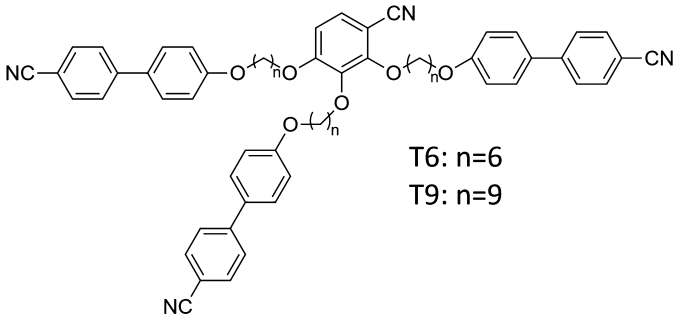

Fig. 1. Chemical structure of the asymmetric trimeric 'tripod' liquid crystal 2,3,4-tris[n-(4-cyanobipheny-4'-yloxy)alk-1-yloxy]benzonitriles. Sample T6 corresponds to $n = 6$ and sample T9 to $n = 9$.

We here present a detailed investigation of the temperature dependent molecular relaxations in two tripod liquid crystals differing only in the alkyl spacer length of their arms, corresponding to either six or nine carbons. The phase behaviour and dielectric properties as well as the full molecular relaxation dynamics of these two tripods were investigated using broadband dielectric spectroscopy (BDS), differential scanning calorimetry (DSC), small amplitude oscillatory shear (SAOS) rheology and steady state shear rheology. We characterise the detailed T-dependent behaviour of the observed α, δ, β, and γ relaxations. We particularly investigate the dynamic crossover observed for the α relaxation time, which we compare with the behaviour observed both for other LC-systems including SCLCPs, and non-LC glass-formers. Moreover, we investigate how the transport of ions in the tripods is linked to the relaxation dynamics.

2. Materials and methods

2.1. Tripod liquid crystals

The two LC tripods: 2,3,4-tris[*n*-(4-cyanobiphenyl-4'-yloxy)alk-1-yloxy] benzonitriles, are denoted as Tn, where n is either 6 or 9; see the chemical structure in Fig. 1. Tn are asymmetric tripods derived from 2,3,4-trihydroxy benzonitrile, which in turn is connected to three cyanobiphenyl arms via ether linkages with alkyl spacers of different lengths. The tripods were synthesised according to Srinatha et al. [24]. In previous studies it has been demonstrated that Tn LCs form intercalated nematic phases without cybotactic clustering [24,25]. The phase behaviour of T6 and T9 were determined using DSC and polarised optical microscopy (POM), as outlined below. The phase sequence and the corresponding transition temperatures, as obtained from POM for T6 are: G 294 K N 408 K Iso, and for T9: G 287 K N 378 K Iso. The DSC traces obtained for two successive heating and cooling cycles, all carried out at the rate of 10 K/min, are shown for both T6 and T9 in figure S1 in the Supplementary Information (SI).

2.2. Differential scanning calorimetry

DSC experiments were performed using a TA Instruments Q2000 heat flux DSC in combination with a liquid nitrogen cooling system. For all DSC runs, ~7.5 mg of sample was placed in an aluminium Tzero hermetically sealed pan. Rate-dependent DSC was performed by cooling the sample across the glass transition region at rates of 1-50 K/min. In addition to this, temperature-modulated DSC (TMDSC) experiments were performed by applying a sinusoidal temperature profile to a linear heating ramp across the glass transition region. Three different temperature profiles were chosen: modulation periods of 40, 60, and 100 s; with modulation amplitudes of 0.8, 1.2, and 2 K; and linear heating ramps of 1.25, 0.83, and 0.5 K/min, respectively. These parameters were chosen such that the heat flow as a result of the modulation (the so-called reversing heat flow), and the number of oscillations over the α relaxation temperature window were consistent between the three different modulation periods. 6-10 modulation periods occur within the glass transitions temperature range (shown in figure S2) such that the material remains quasi-isostructural across a single modulation [73]. For all DSC and TMDSC measurements, T_g was defined by the fictive temperature determined using the technique outlined by Moynihan et al. [74].

2.3. Polarised optical microscopy

For POM experiments (the same cells were subsequently used for dielectric spectroscopy), 20 μm planar aligned liquid crystal cells with ITO electrodes (15Ω/m^2, AWAT, Poland) were used; the cells contained SE130 polyimide alignment layers rubbed antiparallel (top and bottom substrate rubbed in opposite directions). For optical determination of the LC phases, unaligned glass cells were fabricated in order to observe the unaligned texture of materials. The unaligned cells used for POM experiments were fabricated in-house with a cell gap of 11 μm. All cells were filled in the isotropic phase of the LCs.

2.4. Birefringence

The birefringence, Δn, of T6 and T9 were measured using a Berek compensator. The T-dependent birefringence of T6 and T9 were fitted using:

$$\Delta n(T) = (\Delta n)_0 \left(1 - \frac{T}{T_c}\right)^{\Lambda}, \tag{4}$$

where $(\Delta n)_0$ is the birefringence at zero Kelvin, T is the temperature, T_c a temperature just above the isotropic-to-nematic phase transition temperature and Λ is a material constant with a value between 0.15 and 0.2. [75].

2.5. Broadband dielectric spectroscopy

Broadband dielectric spectroscopy (BDS) was performed using a Novocontrol Alpha-A dielectric analyser and covered a frequency range of 30 mHz to 2 MHz, using an AC RMS voltage of 0.4 V. The liquid crystal cells, described above, were used for the experiments and the temperature was controlled using a Novocontrol Quatro cryosystem with an accuracy of 0.1 K. The samples were first heated to their isotropic phase, and subsequently cooled to 113 K (within the glass) using a cooling rate that varied between 10-15 K/min. The frequency (f) dependent complex permittivity data $\varepsilon^*(f)$ were described using a sum of a powerlaw loss contribution from the ITO electrodes, a loss contribution from ionic DC-conductivity, and a set of contributions from the observed molecular relaxations, each described by either a Havriliak-Negami (HN) [76], or a Cole-Cole (CC) [77] expression:

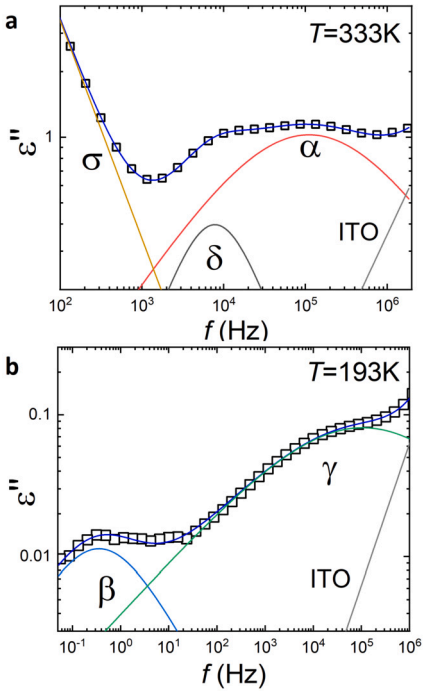

Fig. 2. The dielectric loss as a function of frequency for T6 at (a) 333 K (nematic phase) and (b) 193 K (glassy phase). The different contributions to the dielectric loss are shown, including the ionic dc-conductivity (σ), the δ relaxation, the structural α relaxation, the β relaxation, the γ relaxation, and the contribution from the ITO electrodes. The detailed fitting approach is described in detail in the text.

$$\varepsilon^*(\omega) = A_{\mathrm{ITO}}\omega^{n_{\mathrm{ITO}}}i - \frac{\sigma_{\mathrm{DC}}}{\varepsilon_0\omega}i + \sum_{j=\delta,\alpha,\beta,\gamma}^{N}\frac{\Delta\varepsilon_j}{(1+(i\omega\tau_{HN,j})^{a_j})^{b_j}} + \varepsilon_\infty. \quad (5)$$

Here, σ_{DC} is the DC-conductivity and A_{ITO} is the amplitude of the ITO electrode powerlaw contribution; N is the number of relaxation processes contributing to the data, the index j refers to a specific relaxation, ε_∞ is the high-frequency limit of the dielectric permittivity, $\Delta\varepsilon_j$ is the dielectric strength, and $\tau_{HN,j}$ is a characteristic relaxation time for relaxation j; a_j and b_j are parameters that describe the breadth and asymmetry of the jth relaxation process. For both T6 and T9, four molecular relaxations were observed within the investigated temperature range. In addition to the structural α relaxation, a slower δ relaxation and two faster sub-glassy relaxations, here termed β and γ, were observed within the experimental window, where we have used the same relaxation nomenclature as often used for SCLCPs (see e.g. [61]). For the α relaxation the a parameter varied between 0.5 and 0.7 while the b parameter varied between 1 and 0.6. The δ process could be well described as a Debye relaxation where the a and b parameters are set to 1, while the β, and γ relaxations required a Cole-Cole fitting function where b was set to 1 while a varied between 0.4 and 0.7 for the β relaxation, and between 0.5 and 0.2 for the γ relaxation. Fig. 2 shows examples of the fitting for the T6 sample, both in the liquid nematic state at $T = 333$ K, and the glassy state at $T = 193$ K.

Throughout this paper, we use the time-scale characterising the maximum of the dielectric loss τ_p, which corresponds to the most probable relaxation time, as the characteristic relaxation time for a particular relaxation. For asymmetric relaxation processes, i.e. where $b \neq 1$, τ_{HN} does not correspond to either the loss peak maximum, or the average relaxation time. Thus, to obtain τ_p we use the expression [32]:

$$\frac{1}{\tau_p} = \frac{1}{\tau_{HN}}\left[\sin\left(\frac{a_j\pi}{2+2b_j}\right)\right]^{1/a_j}\left[\sin\left(\frac{a_jb_j\pi}{2+2b_j}\right)\right]^{-1/a_j}. \quad (6)$$

The ITO electrodes show a temperature-independent contribution to the dielectric loss at high frequencies, as shown in Fig. 2. To verify that the observations for the tripods are not significantly influenced by the choice of ITO electrodes, we also performed experiments on an unaligned sample of the tripod T6 using brass electrodes. For these experiments, 10 mm circular brass plates were used with a sample thickness of 50 μm.

2.6. Rheology

2.6.1. Small amplitude oscillatory shear rheology

Small amplitude oscillatory shear (SAOS) rheology was performed on the LC tripod T6 using a Rheometrics ARES strain-controlled rheometer. The sample temperature was controlled using a liquid nitrogen cooling system controlling a forced convection oven. 5 mm diameter plates in a parallel plate geometry were used with a sample thickness of 1.35 mm at $T = 333$ K. The sample thickness was gradually reduced for lower temperatures (due to the sample density increase) to maintain a constant sample radius, resulting in a sample thickness of 1.15 mm at $T = 289$ K. Strain sweep measurements were conducted to confirm that the measurements were performed in the linear viscoelastic regime and the strain amplitude was varied with temperature, ranging from 10% at $T = 333$ K to 0.03% at $T = 289$ K.

Time Temperature Superposition (TTS) can often be used to combine data sets for individual temperatures into a mastercurve. However, the use of TTS is only relevant when the data for a specific temperature range are controlled by the same relaxation process [78]. To investigate the relevance of a TTS analysis, the loss tangent $\tan(\delta)$ is plotted versus the absolute complex modulus $|G^*|$ in a so-called van Gurp Palmen (vGP) plot in figure S10 (SI). The explicit time-dependence is removed from the data in this representation and the plot thus demonstrates whether a TTS mastercurve can be produced simply by application of a horizontal frequency shift-parameter. As shown in figure S10 (SI), the vGP plot shows two regions where the data collapse well; one in the high modulus low T range, and one in the low modulus high T range. This behaviour with two, or more, separate T-dependent relaxations is commonly observed due to the existence of chain modes or phase changes in the material [79–82]. Thus, we conclude that the low and high T data are dominated by two different relaxation processes and two separate master curves, one for each region, were thus produced.

2.6.2. Steady state shear rheology

The shear viscosity was determined for the T6 sample using an Anton Paar MCR 302 stress-controlled rheometer. A parallel plate geometry was used with 25 mm diameter plates and a sample gap of 0.11 mm; the sample gap was monitored using Anton Paar's TruGap feature. Measurements were performed within a temperature range of 333 - 418 K, to encompass both the isotropic and nematic states.

3. Results

3.1. Optical and phase behaviour

Both T6 and T9 demonstrate a wide temperature range nematic phase: T6 shows a nematic phase between 408 K and 294 K and T9 exhibits a nematic phase between 378 K and 287 K; for lower temperatures, each sample vitrifies and forms a nematic glass where the T_g given here is defined by the onset temperature as determined from DSC. The enthalpy of the isotropic to nematic transition is 3.44 kJ/mol for T6 and 3.77 kJ/mol for T9. The nematic phase is enantiotropic in both materials. The materials showed no hysteresis effects and the glass states were accessible during both cooling and heating cycles for all investigated rates. Fig. 3b shows the typical Schlieren texture of the nematic phase of sample T6 observed using POM. In planar rubbed cells, both T6 and T9 shows good homogeneous alignment (Fig. 3b) throughout the nematic phase. The T-dependence of the birefringence for samples

Table 1
VFT parameters from the fits of α and δ relaxation data for samples T6 and T9, as determined from BDS experiments.

	T6				
	T_g (K)	$\log(\tau_0)$ (s)	T_0 (K)	D	m
δ Process	294	-9.33 ± 0.06	266.5 ± 0.6	2.65 ± 0.07	120 ± 30
α Process	294	-10.67 ± 0.07	270.5 ± 0.4	2.57 ± 0.05	160 ± 40
	T9				
	T_g (K)	$\log(\tau_0)$ (s)	T_0 (K)	D	m
δ Process	287	-8.4 ± 0.1	268.3 ± 0.8	1.70 ± 0.08	160 ± 60
α Process	287	-9.79 ± 0.04	269.8 ± 0.2	1.78 ± 0.02	190 ± 30

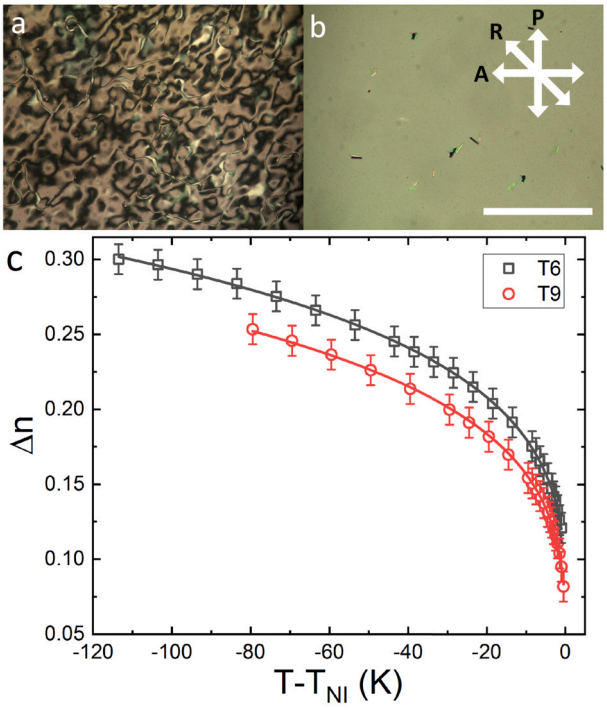

Fig. 3. POM images of sample T6: (a) between glass plates with no alignment layer at $T - T_{NI}$ =28.5 K showing the Schlieren texture characteristic of a nematic phase; (b) filled into a 10 μm planar cell. P, A and R refer to the polariser, analyser and rubbing directions, respectively. The scale-bar corresponds to 200 μm. (c) Plot of the temperature-dependent birefringence of T6 (black squares) and T9 (red circles) within their nematic phase. The solid lines are the results of fits to eq. (4), as described in the text.

T6 and T9 are shown in Fig. 3c; at $T - T_{NI}$ = -110 K, T6 shows a birefringence of 0.3 and at $T - T_{NI}$ = -80 K, T9 shows a birefringence of 0.25. For comparison, the commonly used cyanobiphenyl-based calamitic liquid crystal 5CB has a birefringence of 0.22 [83] at $T - T_{NI}$ = -22 K. Thus, as expected, at room temperature, both T6 and T9 has higher birefringence than 5CB; higher birefringence LC components are desirable for many applications such as displays and telecommunication devices [84]. Even though a clear glass transition was observed in DSC data for both T6 and T9 (figure S1 in the SI), no significant textural or optical birefringence changes were observed at the glass transition.

3.2. Broadband dielectric spectroscopy

BDS measurements of the complex dielectric permittivity were carried out in a planar aligned cell. Representative frequency sweeps of the dielectric loss for selected temperatures are shown in Fig. 4 for both T6 and T9. In the nematic phases of both T6 and T9, the α and δ relaxations are observed. An example of the fitting of the nematic liquid state is shown for sample T6 in Fig. 2a, where the contributions to the dielectric loss from DC-conductivity, the δ, and α relaxations, as well as the ITO electrode contributions are shown at a temperature of 333 K. As the temperature within the nematic phase is reduced and the glass transition is approached, the δ and α relaxations merge into one effective single relaxation process, as shown in Fig. 4a. The merging of the two relaxation processes as T_g is approached from above is similar to the behaviour typically observed in SCLCPs [30,31,64–66]. Figure S6 (SI) shows the ratio of the δ and α relaxation times for both the T6 and T9 samples, demonstrating that the timescale separation for both relaxation processes, and thus the and merging near T_g, is analogous for both materials.

In the glassy state of both T6 and T9, two further secondary relaxation processes are observed; these are observed at higher frequencies than the δ and α relaxations. We refer to the slower of these two secondary relaxations as the β process and the faster as the γ process, following nomenclature common in the literature for SCLCPs [61] (see Fig. 2b).

The temperature-dependent relaxation times for the four observed relaxations are shown in Fig. 5 in Arrhenius plots. It is clear that both T6 and T9 show similar qualitative behaviours for all four observed relaxation processes. The relaxation times of the δ process can be described in its entirety using a VFT expression (2). The α process can also be well-described using a VFT expression for temperatures near T_g. From the VFT parameters, T_g for T6 and T9 were determined as 294 K and 287 K, respectively, in good agreement with the DSC results of 294 K and 287 K (for a heating rate of 10 K/min) for T6 and T9 respectively. A reduction in T_g as the spacer length is increased is consistent with observations for SCLCPs [64]. However, above a temperature T^* (T^* = 335 K for T6 and T^* = 325 K for T9, as marked in black vertical dashed lines in Fig. 5, $\tau_\alpha(T)$ is instead best described using an Arrhenius behaviour. Dielectric loss spectra around this transition point are shown in figure S3. The VFT and Arrhenius fitting parameters for the δ and α processes are shown in Table 1.

Further evidence for changes in dynamics near T^* can be found from the HN fitting parameters corresponding to the δ and α processes, respectively, as shown in figure S4 (SI). Figure S4a (SI) and S4b (SI) show the dielectric strength, $\Delta\varepsilon$, versus the ratio T_g/T for the δ and α processes, respectively. For both T6 and T9, the dielectric strength of the δ process, $\Delta\varepsilon_\delta$, decreases as the temperature decreases, whereas the strength of the α process, $\Delta\varepsilon_\alpha$ initially decreases, but then begins to increase around T^*. The HN shape parameters (a and b in equation (5)) are included in figure. S2c (SI), and we find that changes to the T-dependence of the shape parameters of the α process can also be observed at T^*; above T^*, b_α is equal to 1, but for $T < T^*$ b_α decreases.

Both T6 and T9 are highly fragile glass formers with fragilities of m = 160 and m = 190 for T6 and T9 respectively. The high values of fragility for T6 and T9 fall within a range observed for many high molecular weight polymers [47,55,56,85]; it has also been shown that bulky pendant groups appended to the polymer backbone can also create highly fragile glass formers [86].

For $T < T_g$, only the β and γ processes are observed and the T-dependent HN fitting parameters for the β and γ processes are shown

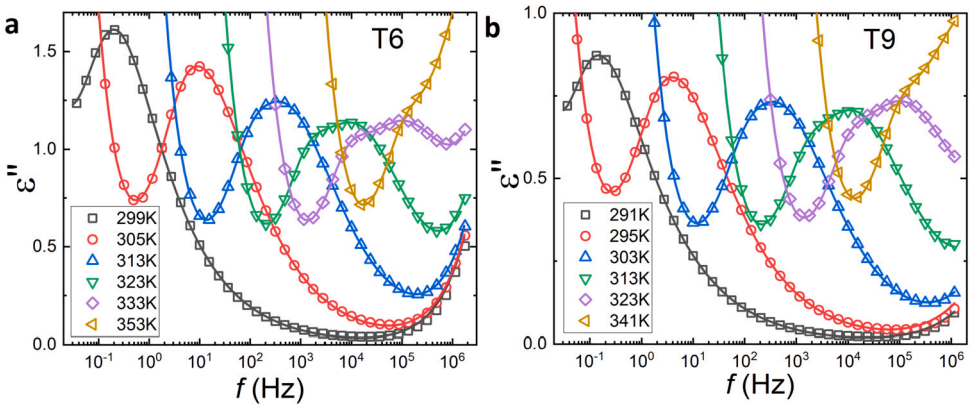

Fig. 4. Representative plots of the frequency-dependent dielectric loss for (a) T6 and (b) T9, both within the nematic state. Two relaxation contributions are observed for both T6 and T9, particularly at the higher temperatures. The two relaxation merge into one effective relaxation for temperatures near the glass transition. T_g for T6 is 294 K and for T9 287 K. The solid lines represent the fit resulting from fitting to Eq. (5).

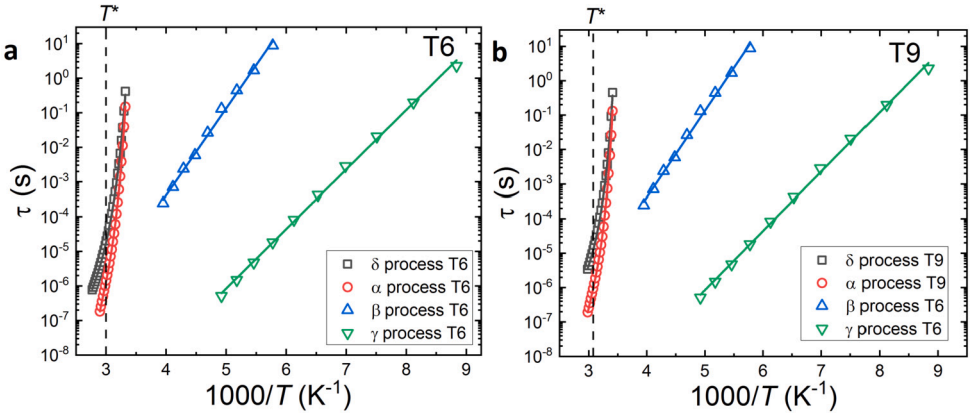

Fig. 5. Arrhenius plots for sample (a) T6 and (b) T9, showing the T-dependent characteristic relaxation times for the δ, α, β and γ relaxations, respectively. The characteristic α and δ relaxation times are well-described near T_g using a VFT equation. However, for $T > T^*$, the α relaxations are best described using an Arrhenius expression. The β and γ relaxations observed within the glass are well-described using Arrhenius expressions. The fits to either VFT or Arrhenius expressions are shown in solid lines.

Table 2
Arrhenius parameters for samples T6 and T9 from the fits of the α relaxation (for $T > T^*$) and β and γ relaxations (for $T < T^*$), as determined from BDS experiments.

	T6		T9	
	$\log(\tau_0)$ (s)	ΔH (kJ/mol)	$\log(\tau_0)$ (s)	ΔH (kJ/mol)
α Process	-31.66 ± 0.03	164.8 ± 0.2	-28.6 ± 0.02	140 ± 1
β Process	-13.4 ± 0.3	48 ± 1	-17.0 ± 0.3	63 ± 1
γ Process	-14.75 ± 0.09	33.1 ± 0.3	-15.7 ± 0.2	36.8 ± 0.5

in figure S5 (SI), as shown for sample T6 at $T = 193$ K in figure 2b. The relaxation times for the β and γ relaxations can be well described using an Arrhenius temperature dependence for both T6 and T9, and the corresponding fitting parameters are provided in Table 2. The dielectric strength $\Delta\varepsilon_\gamma$ shows a slight T dependence for the γ process, decreasing slightly with decreasing temperature, whilst the strength of the β process $\Delta\varepsilon_\beta$ stays almost constant. Since the β and γ processes are symmetric (on a logarithmic abscissa), $b_\beta = b_\gamma = 1$ and only the T-dependencies for a_β and a_γ are relevant. We find that the β process becomes successively narrower over the investigated T-range, whereas the γ process becomes broader.

The activation enthalpies measured for the β and γ relaxations of T6 and T9 are consistent with those observed for SCLCPs of similar spacer length [65,70–72]. Also, for both the β and γ relaxations, we observe a higher activation energy as the tripod arm length is increased. For SCLCPs, the increase in activation energy of the β relaxation, observed for increasing spacer length, is often linked to the formation of higher order LC phases, such as the smectic A, B or C phases [65]. However, our LC tripods form a nematic phase regardless of spacer length [24,25], excluding a direct link between the variation in activation enthalpy and the phase behaviour.

The use of ITO electrodes for measuring the dielectric properties of LC materials is common due to the high optical transparency of ITO and the ease of applying alignment layers to ITO. Thus, with ITO electrodes it is relatively straightforward to achieve uniform alignment and optically verify the alignment quality compared with the situation using opaque electrodes. Since ITO electrodes show a (temperature-independent) high-frequency contribution to the dielectric loss, we also verified the key results by dielectric experiments on an unaligned T6 sample using brass electrodes Figure S7 shows the resulting relaxation

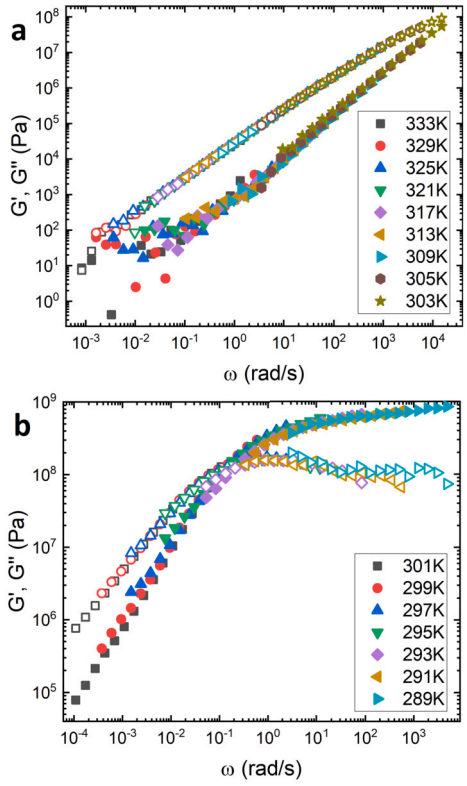

Fig. 6. Mastercurves for sample T6 showing (a) re-scaled data for the dynamic range controlled mainly by the δ relaxation, and (b) re-scaled data for the dynamic range controlled mainly by the α relaxation. For both plots, the closed symbols represent G' and the open symbols G''.

time-scales obtained using brass electrodes, and figure S8 shows the corresponding HN fitting parameters. Moreover, Table S1 shows the fitting parameters for the VFT fits to the α and δ relaxation times-scales and Table S2 shows the fitting parameters for the high-temperature Arrhenius fit of the alpha relaxation data. We find that although the dynamic crossover is less pronounced in the study using brass electrodes, the crossover is still clearly visible and generally there is good agreement between the fitting parameters of the investigations of the aligned sample using ITO electrodes and the unaligned sample using brass electrodes. The discrepancies between the two data sets for the T6 sample, e.g. observed in the high-temperature Arrhenius parameters, are likely due to the lack of alignment in the brass electrode measurements leading to a non-uniform molecular orientation across the sample.

3.3. Small amplitude oscillatory rheology

To further investigate the T-dependent relaxation behaviour, small amplitude oscillatory shear (SAOS) rheology was carried out on the T6 sample within the T range 289 - 333 K. The complex shear modulus $G^*(\omega)$ data are shown in figure S9 (SI) for a range of temperatures within the range 289 - 333 K. As demonstrated by the vGP plot in figure S10 (SI), we find that the SAOS data are mainly controlled by the α relaxation at low T and the δ relaxation at higher T, and we thus split the data into two parts to directly reflect the two relaxation mechanisms and thus produce two separate mastercurves, as shown in 6; here, the reference temperature used was 321 K for the δ process and 295 K for the α process. In Fig. 8, the resulting shift factors, corresponding to the α and δ relaxation data, are scaled onto the characteristic α and δ relaxation time data obtained from BDS, as shown in Fig. 7. We find excellent agreement further confirming the T-dependent relaxation behaviour for the two relaxations.

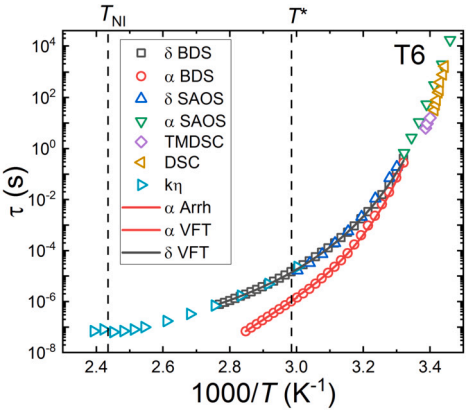

Fig. 7. The characteristic relaxation time τ versus inverse temperature for the α and δ relaxations for sample T6. Data obtained from BDS, SAOS and steady state shear rheology, DSC and TMDSC are shown in symbols outlined in the legend. The relaxation times determined from BDS and TMDSC were determined, as described in the text. The DSC data determined for varying measurement rates were scaled onto the TMDSC data using a shift factor. The shift-factors resulting from the SAOS TTS analysis and the steady state shear viscosity data were scaled onto the BDS relaxation data, to facilitate a direct comparison. The dash-dotted vertical line indicates the isotropic to nematic phase transition temperature T_{NI} obtained from DSC, while the vertical dashed line indicates the temperature at which the temperature-dependence of the alpha relaxation changes from Arrhenius to VFT behaviour. The solid lines are fits to the VFT expression and the dashed line to the Arrhenius expression, as further discussed in detail in the text.

3.4. Steady state shear rheology

The T-dependent steady-state shear viscosity was measured using a stress-controlled rheometer. Stress-strain measurements were performed for the T-range of 333 - 418 K (covering both the isotropic and nematic phases) for the T6 sample, as shown in figure S11 (SI). Newtonian behaviour was observed for all measured temperatures. The measured T-dependent shear viscosities $\eta(T)$ are shown in Fig. 7, where a scaling factor has been applied to compare it to the SAOS and BDS data. We find that the re-scaled $\eta(T)$ corresponds well to the T-dependence of the characteristic relaxation times for the δ relaxation, as shown in Fig. 7. Given the similar T-dependencies, we conclude that $\eta(T)$ and $\tau_\delta(T)$ are coupled, which makes sense given the importance of the significant mesogen movements involved in the δ relaxation for liquid flow.

3.5. Calorimetry

Temperature modulated DSC (TMDSC) experiments were performed on the T6 sample for three different modulation periods, P: 40, 60 and 100 s across the α transition. The transition temperature was defined as the inflection point of the reversing heat capacity step for each modulation period. This yielded the transition temperature at the timescale defined by the modulation period, P, using $\tau_\alpha = P/2\pi$ [87].

Since the time-scales probed by the TMDSC measurements is known, we can use the TMDSC data to determine the characteristic time-scales associated with the applied cooling rates in the standard DSC data. Standard calorimetry data was collected over a wider dynamic range using cooling rates ranging from 1 to 50 K/min. We determine the fictive temperature (determined using the technique outlined in [74]) for the heat flow step corresponding to each cooling rate R, and using $\tau_\alpha = A/R$, with the constant A tuned to provide overlap with the TMDSC data to extend the investigated dynamic range, as shown in Fig. 7. In summary, we find that the complementary experimental techniques provide a consistent picture with two main relaxations for $T > T_g$, the δ and α relaxations, which approach and effectively merge near T_g.

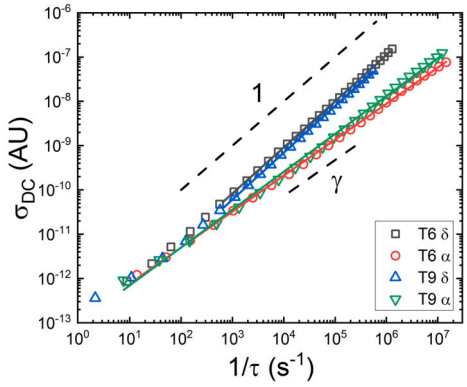

Fig. 8. Double-logarithmic plot of the ionic DC-conductivity versus the inverse of either the α or δ relaxation time for samples T6 and T9. The solid lines are fits with powerlaw expressions ($\sigma_{DC} = \tau^{-\gamma}$), where the slope of the line (γ) indicates the degree of decoupling between the DC-conductivity and the corresponding relaxation. The black dashed line has a slope of 1 ($\gamma = 1$), thus corresponding to fully coupled behaviour. The values of γ for the α and δ processes respectively are: 0.81±0.05 and 1.04±0.05 for T6, and 0.86±0.05 and 1.06±0.05 for T9.

3.6. Ion transport

There is significant interest in better understanding how to control and enhance ion transport in materials. Important examples include materials for energy storage such as Li-ion batteries where both the electrolyte and electrode binders need efficient ion transport [88,89]. Polymer-based ion-conducting electrolytes are particularly interesting since they could provide rigidity, flexibility, and safety to batteries. However, since the motion of ions typically requires a degree of structural relaxation, and for macromolecules such as polymers, the structural relaxation is relatively slow, the ion transport of polymers is often not sufficiently efficient for many applications [90,91]. One route to address this is to add plasticizers that speed up the structural relaxation, and thus increase the conductivity. However, the additives typically affect the safety and electrochemical properties of the materials. Thus, it is important to understand how pure polymeric, and oligomeric, materials operate in terms of ion transport, and particularly how to decouple ion transport from the structural relaxation.

The degree of decoupling can be quantified from the relationship $\sigma_{DC} \propto \tau_\alpha^{-\gamma}$, where σ_{DC} is the T-dependent DC-conductivity, τ_α is the structural relaxation time, and γ is a parameter which quantifies how similar the T-dependencies are; a value of $\gamma \approx 1$ means that the two show the same T-dependence, whereas a value significantly lower than 1 indicates strong decoupling. Most long-chain polymers demonstrate decoupling near T_g, i.e. $\gamma < 1$ [90] and a rough trend has been observed, where more fragile polymers typically demonstrate a stronger decoupling. This trend was originally suggested to be related to the fact that fragile polymers typically pack less effectively, leaving more space for ions to move, and thus relying less on structural relaxation for ion transport to take place [90].

Polymeric, or oligomeric, systems with LC functionalities have been identified as interesting for applications, e.g. as battery electrolytes, where ion transport is key [92,93]. Most of this work relies on the LC phase providing effective channels for ions to move through [93–96], whereas much less is known about the connection between ion motions and structural relaxation in LC systems. A decoupling of ion transport from the structural α relaxation has been observed for a SCLCP [97]. We also note that it has been suggested for a non-LC side-chain polymer that ion transport may couple to motions of the side chains [98]. Several studies have investigated this for nematic LC systems [33,34,37] and for 5CB a deviation from $\gamma = 1$ was observed as T_{NI} was approached, which was interpreted as due to the presence of pre-transitional nematic fluctuations [35]. In another study, it was shown that nanoparticles added to 5CB reduced this decoupling and this was interpreted as due to nanoparticle-induced disruption of the pre-transitional fluctuations [37]. Moreover, in a recent study on a liquid crystalline elastomer (LCE), which could be prepared in chemically identical nematic or isotropic phases through cross-linking, a significantly higher decoupling was observed in the nematic than in the isotropic LCE phase, which was also suggested to be related to differences in pre-transitional and nematic fluctuations, and in the corresponding difference in dynamic heterogeneity between the two phases [68].

Tripod LC materials are a type of LC materials for which very little is known about ion transport. In this study, we have not specifically added ions. However, a small level of ionic impurities present in the samples makes it possible to determine the T-dependent ion conductivity, and to link this to the observed molecular relaxation processes. To investigate how the T-dependence of $\sigma_{DC}(T)$ compares with the T-dependence of the α and δ relaxations, which are observed within the same T-range, we plot $\sigma_{DC}(T)$ versus $\tau_\alpha(T)$ in a double-logarithmic Walden-like plot 8; a gradient of unity in this type of plot demonstrates that the T-dependencies are the same and thus suggests a direct relationship.

We find for both T6 and T9 that near T_g, where the α and δ relaxations are merged, the DC-conductivity is decoupled from the merged relaxation, as represented by $\gamma < 1$. For higher T, as the α and δ relaxations separate, we find that σ_{DC} continues to be decoupled from $\tau_\alpha(T)$, as demonstrated by the γ values of 0.81 ± 0.05 for T6 and 0.86 ± 0.05 for T9, respectively. However, in this dynamic regime, σ_{DC} follows the T-dependence of the δ relaxation well and the corresponding γ values are 1.04±0.05 and 1.06±0.05 for samples T6 and T9, respectively; we expect any slight difference from unity here to be due to the increasing difficult of fitting the δ and α relaxations near T_g. We note that, as shown for sample T6 in Fig. 7, the δ relaxation has the same T-dependence as the shear viscosity $\eta(T)$. Thus, the ion motions are well coupled to the shear viscosity. For simpler liquids, the shear viscosity and the structural α relaxation are typically related through $\eta(T) = G_\infty(T)\tau_\alpha(T)$, where the instantaneous shear modulus $G_\infty(T)$ has a weak T-dependence and η is thus approximately proportional to τ_α.

For the tripods, our results suggest that for temperatures where the δ relaxation is active, and thus the re-orientations of the mesogen arms takes place on the relevant time-scales, the ions utilise the motion of the tripod arms to move through the liquid. As shown for the chemical structure of the tripods (see Fig. 1), ionic coordination sites are situated both at the end of the mesogen arms (cyano group), at its centre, and on either side of the alkyl spacer (oxygens). Thus, it is feasible that the movement of the tripod arms plays an important role in the ion transport.

Finally, we note that systems for which significant ion conduction requires the motion of tripod arms (or side-chains for SCLCPs) are interesting due to the possibility of tuning the ionic transport properties by design of the properties of the arms, such as their length and flexibility, as well as the number and location of the ion coordination sites. Understanding the mechanisms behind ion transport in systems such as these is important for the functional design of new materials with well controlled ion transport.

4. Discussion

We reiterate the observed change from VFT to Arrhenius behaviour observed at T^* for the α relaxation, as shown in Fig. 7; the temperature T^* corresponding to this 'dynamic crossover' is marked by a vertical black dashed line. To further investigate this crossover, we plot the data in a representation which linearises a VFT behaviour and identifies changes in the behaviour. We calculate the linearisation parameter Z [99],

$$Z = \left(\frac{d\log(\tau_i)}{d(1000/T)}\right)^{-1/2} = \left(\frac{DT_0\log(e)}{1000(\frac{T_0}{T}-1)^2}\right)^{-1/2}, \quad (7)$$

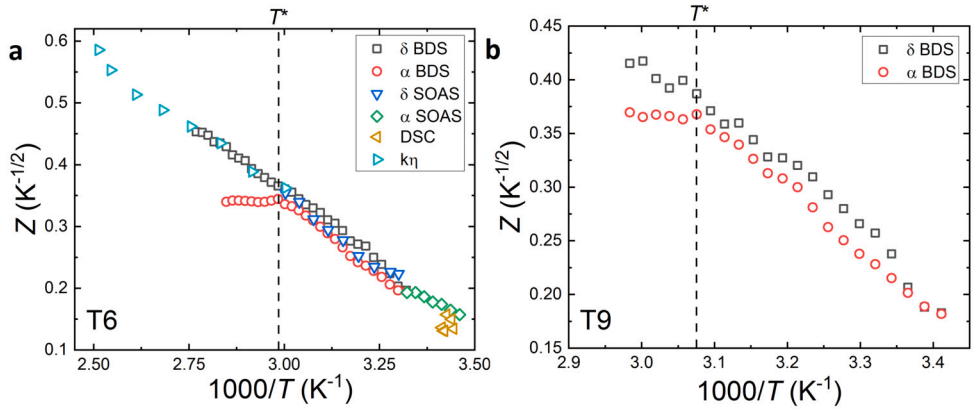

Fig. 9. Derivative analysis for **a)** sample T6 and **b)** sample T9, for the data sets outlined in the legend. The vertical dashed line marks the temperature T^* for which the alpha relaxation changes temperature dependence from VFT ($T < T^*$) to Arrhenius ($T > T^*$).

where τ_i represents either the α or the δ relaxation processes, and plot Z versus inverse temperature in Fig. 9. The slope of the linear behaviour in the resulting plot provides a measure of how non-Arrhenius the behaviour is; a steep slope corresponds to a highly non-Arrhenius behaviour, whereas a zero slope corresponds to an Arrhenius behaviour. Linearization plots for both the T6 and T9 samples are shown in Fig. 9a and Fig. 9b, respectively. For both samples, we find that the δ process can be well described using a VFT expression over the full investigated T-range, whereas the α relaxation changes from a VFT to an Arrhenius behaviour for $T > T^*$, where $T^*/T_g = 1.14$ and $T^*/T_g = 1.13$ for T6 and T9 respectively. Moreover, it is clear that the VFT behaviour is very similar for the δ and α relaxations near T_g; this is further confirmed by the VFT fitting parameters, shown in Table 1.

A similar dynamic crossover from VFT to Arrhenius behaviour [26,30,31,63–66,100] (typically observed for a ratio $T^*/T_g \approx$ 1.1-1.2) as well as δ and α relaxations merging near T_g, are also commonly observed [30,31,64–66] for SCLCPs. The T-dependence of the δ relaxation has either been reported as non-Arrhenius (typically described by a VFT expression) [100,101], or as Arrhenius, where the full dynamic range is often associated with two separate Arrhenius behaviours, each characterised by a different activation energy [30,31,64,66,101]. However, for the latter behaviour, the temperature characterising the dynamic change is generally different from T^*. Thus, both the observations for SCLCPs of a merging of the α and δ relaxations near T_g, and the presence of a dynamic crossover at T^* are consistent with the behaviour of the tripods.

Several different interpretations of the dynamic crossover at T^* in SCLCPs have been suggested in literature. One commonly invoked interpretation is that T^* is related to the presence of microphase separation, leading to mesogen-rich and backbone-rich layers [102]. As the temperature is reduced towards T_g, the molecular motions involved in the structural relaxation become more correlated; thus, the corresponding characteristic length-scale grows and eventually approaches the length-scale characteristing the phase-separation-driven meso-scale structure, which should lead to changes in the relaxation behaviour [65]. However, an SCLCP in the smectic-E phase has shown compact layers with relatively short inter-layer distances [67,103,104], and for the SCLCP in the smectic-E phase a dynamic crossover characterised by a low-T Arrhenius and a high-T VFT behaviour has been observed [67]. This has often been interpreted as due to nano-confinement, where the fixed activation energy of the Arrhenius behaviour is linked to the confinement length-scale [105,106]; this interpretation is different from the suggestion that the Arrhenius to VFT transition is due to microphase separation (see discussion above) in another work on SCLCPs by Schönhals et al. [65]. For the tripods T6 and T9, the X-ray scattering data recently reported by Srinatha et al. do not show any evidence for nano phase separation [24], and we thus do not consider any nano- or microphase separation effects a plausible explanation for our tripods. For some SCLCP materials, T^* has been reported to coincide with changes in phase behaviour, such as: isotropic to nematic [31], isotropic to smectic A [66], or nematic to smectic [30] but this also is not a plausible explanation for our tripods as no evidence of a phase transition in the region of T^* has been detected in the optical, calorimetry or X-ray scattering data recently reported by Srinatha et al. [24].

A study by Schönhals et al. [64], where both SCLCPs and chemically analogous isotropic side-chain polymers were investigated, suggests that the presence of an LC phase is necessary to observe the change in dynamics from a low-T VFT to a high-T Arrhenius behaviour at a crossover temperature T^*. In this study the isotropic side-chain polymer were well-described by the same VFT behaviour throughout. The study also showed that T^* decreases with increasing mesogen spacer length, whereas the ratio T^*/T_g remains roughly constant varying between 1.10-1.15 for varying spacer lengths, suggesting that the origin of the crossover behaviour is linked to the glass transition behaviour, and thus T_g. A similar conclusion was also recently reached for an LC elastomer, which could be produced both in a nematic and isotropic state. For this system, the dynamic transition behaviour could not be linked to any phase-separation [68]. Instead, the crossover between Arrhenius and VFT behaviour observed for $\tau_\alpha(T)$ was instead attributed to a matching between the length-scale of correlated molecular motions involved in the α relaxation and the length-scale characterising nematic fluctuations. The transition from VFT to Arrhenius was only observed for the nematic elastomer, whereas the isotropic elastomer instead showed a transition from a VFT (at low-T) to another VFT (less fragile), and the characteristic size of correlated motions at T^* was found to correspond to the size characteristic of pre-nematic fluctuations. Thus, this study strongly suggests that for the investigated elastomers the presence of nematic fluctuations is key for the transition to a more Arrhenius-like behaviour at T^*, whereas the presence of a dynamic crossover at T^* signifies more general changes in the liquid behaviour. We also reiterate that glass-formers in general demonstrate a dynamic crossover at a temperature T_B, where the ratio $T_B/T_g \approx 1.2-1.6$ [46,47], and the value of this ratio has demonstrated some correlation with the fragility [47]. Thus, the existence of a dynamic crossover is general for glass-formers, but the transition to a high-T Arrhenius behaviour for a temperature situated so close to T_g appears to require liquid crystal functionality.

Finally, it is worth noting that a dynamic crossover observed in LC dimers displays some similarities to the observations for SCLCPs and our tripod LCs. For LC dimers, three molecular relaxation processes are typically reported [107,108]: two of these are normally assigned to 'flip-flop' motions of the mesogen moieties around the director, referred to as δ processes [109,110], thus consistent with the nomenclature used for our tripods, LC elastomers [68] and SCLCPs [61]. For symmetric dimers, the two δ processes overlap and are indistinguishable [108]. The third observed relaxation process is typically assigned to rotation around the molecular long axis [108,110]. As the glass transition temperature is

approached, the three relaxations approach each other and effectively merge to a single relaxation reaching time-scales of ≈ 100 s at T_g. As one example, the liquid crystal dimer (1,7-bis-4- (4'-cyanobiphenyl) heptane) (CB7CB) consists of two cyanobiphenyl moieties separated by a methylene spacer. This liquid shows both nematic and twist-bend nematic phases, and due to its symmetrical nature, only two relaxation processes are thus observed in its liquid state. Both observed relaxations show VFT behaviours at low temperatures (near T_g) [109] and dynamic crossovers to Arrhenius behaviour at high temperatures [10,111]. The crossover at T^* for CB7CB in the twist-bend phase corresponds to the ratio $T^*/T_g = 1.2$. A similar behaviour has been observed also for a non-symmetric dimer in the smectic A phase [110] demonstrating that the dynamic crossover is not specific to a particular LC phase.

5. Conclusions

In this work, we present the temperature-dependent optical and dielectric properties, the molecular relaxation dynamics, rheological response, and ion transport properties for two cyanobiphenyl-based liquid crystal (LC) tripods, characterised by alkyl tail-lengths of either 6 or 9 carbons for samples T6 and T9 respectively. We demonstrate that both T6 and T9 exhibit a wide temperature range nematic phase ($\Delta T > 90$ K). In addition, the nematic phase in both tripods shows a higher birefringence than what is typically observed for standard calamitic nematic LCs, a useful property for display and telecommunication applications [84]

Using broadband dielectric relaxation spectroscopy, calorimetry, oscillatory and steady state shear rheology, four molecular relaxation processes (α, δ, β and γ) were identified and their corresponding temperature-dependent characteristic relaxation times were mapped out. The β relaxation was assigned to reorientation around the mesogen long axis, and the γ relaxation to internal tripod arm rearrangements. Both the β and γ relaxations were observed in the glassy state where their characteristic relaxation times both showed Arrhenius temperature dependencies with activation energies similar to those previously observed for side-chain liquid crystal polymers (SCLCP) with side-chains of similar lengths as the tripod arms. The δ relaxation was assigned to reorientation of the mesogen unit around its short axis and we find that it follows a non-Arrhenius VFT dependence over the full investigated temperature range.

The structural (α) relaxation defines the glass transition temperature T_g and the fragility i.e. the T-sensitivity at T_g. We find that T6 and T9 have similar T_g values (294 K and 287 K) and fragilities ($m = 160$ and 190), where the fragilities correspond to values typical of polymers [47,55,56]. Importantly, the α and δ relaxations merge on approach of T_g, demonstrating that as the range of correlated motions involved in the α relaxation increases, the motion of the mesogen arm becomes part of the same relaxation event. In this temperature range, the two relaxations can both be well described by the same VFT-behaviour. For higher temperatures, on the other hand, the two relaxations separate and for $T > T^*$, where T^* marks a dynamic crossover, the α relaxation transitions from VFT to Arrhenius behaviour.

Both the T6 and T9 tripods show a ratio of $T^*/T_g = 1.14$ and $T^*/T_g = 1.13$ respectively, which is consistent with the ratio observed for many side-chain LC polymers (and other LC systems). Moreover, the ratio is consistent with that observed more generally for non-LC systems, where a transition between two different VFT behaviours typically takes place for $T^*/T_g \approx 1.2-1.6$ [48,49], and a correlation between the ratio and fragility has been suggested [47]. For non-LC systems, however, the transition to Arrhenius behaviour takes place at significantly higher temperatures relative to T_g. Thus, the presence of LC order leads to significant differences in the characteristic molecular motions and thus the quantitative crossover behaviour.

Finally, we find that for temperatures where the α and δ relaxations separate, the transport of ions for the LC tripods decouples from the α relaxation instead following the δ relaxation. We suggest that this is due to the position of ion coordination sites on the mesogen arm and note that tuning of the ion transport can thus be achieved by the design of the properties of the tripod arms.

CRediT authorship contribution statement

Jordan Hobbs: Conceptualization, Data curation, Formal analysis, Investigation, Methodology, Visualization, Writing – original draft, Writing – review & editing. **Matthew Reynolds:** Formal analysis, Investigation, Methodology, Validation, Visualization, Writing – review & editing. **Mallasandra Krishnappa Srinatha:** Investigation, Methodology, Writing – review & editing. **Govindaswamy Shanker:** Investigation, Methodology, Writing – review & editing. **Johan Mattsson:** Conceptualization, Funding acquisition, Methodology, Supervision, Writing – review & editing. **Mamatha Nagaraj:** Conceptualization, Funding acquisition, Methodology, Supervision, Writing – review & editing.

Declaration of competing interest

The authors declare that they have no known competing financial interests or personal relationships that could have appeared to influence the work reported in this paper.

Data availability

The data in this paper are available in the Leeds Data Repository (https://doi.org/10.5518/1405).

Acknowledgements

J.H. would like to acknowledge Dr Thomas Raistrick and Dr Daniel Baker of University of Leeds for useful discussions. J.H., M.N. and J.M. gratefully acknowledge financial support from the Engineering and Physical Sciences Research Council (EPSRC) funded Centre for Doctoral Training in Soft Matter and Functional Interfaces (grant EP/L015536/1). M.R. and J.M. also thank the EPSRC (EP/M009521/1) for financial support. G.S. thanks Bangalore University, Jnana Bharathi Campus, Bengaluru-560056 for financial support through UNI. ORDER. No. Dev:D2a:BU-RP:2020-2021. S.M.K. thanks DST-SERB for financial support through No. PDF/2022/000321.

Appendix A. Supplementary material

Supplementary material related to this article can be found online at https://doi.org/10.1016/j.molliq.2023.123069.

References

[1] J.C. Jones, The fiftieth anniversary of the liquid crystal display, Liq. Cryst. Today 27 (3) (2018) 44–70, https://doi.org/10.1080/1358314X.2018.1529129.
[2] M. O'Neill, S.M. Kelly, Ordered materials for organic electronics and photonics, Adv. Mater. 23 (5) (2011) 566–584, https://doi.org/10.1002/adma.201002884.
[3] T.R. Woliński, A. Siarkowska, D. Budaszewski, M. Chychłowski, A. Czapla, S. Ertman, P. Lesiak, K.A. Rutkowska, K. Orzechowski, M. Sala-Tefelska, M. Sierakowski, R. Dabrowski, B. Bartosewicz, B. Jankiewicz, E. Nowinowski-Kruszelnicki, P. Mergo, Recent advances in liquid-crystal fiber optics and photonics, in: L.-C. Chien (Ed.), Emerging Liquid Crystal Technologies XII, in: International Society for Optics and Photonics, vol. 10125, SPIE, 2017, p. 101250W.
[4] R. Morris, C. Jones, M. Nagaraj, Liquid crystal devices for beam steering applications, Micromachines 12 (3) (2021), https://doi.org/10.3390/mi12030247, https://www.mdpi.com/2072-666X/12/3/247.
[5] J. Goodby, I. Saez, S. Cowling, V. Görtz, M. Draper, A. Hall, S. Sia, G. Cosquer, S.-E. Lee, E. Raynes, Transmission and amplification of information and properties in nanostructured liquid crystals, Angew. Chem., Int. Ed. Engl. 47 (15) (2008) 2754–2787, https://doi.org/10.1002/anie.200701111, https://onlinelibrary.wiley.com/doi/pdf/10.1002/anie.200701111, https://onlinelibrary.wiley.com/doi/abs/10.1002/anie.200701111.
[6] J. Majnusz, J. Catala, R. Lenz, Liquid crystal polymers—11. Structure-property relationships in a series of thermotropic poly(2-n-alkyl-1, 4-phenylene terephthalates), Eur. Polym. J. 19 (10) (1983) 1043–1046, https://doi.org/

10.1016/0014-3057(83)90070-8, https://www.sciencedirect.com/science/article/pii/0014305783900708.
[7] C.T. Imrie, P.A. Henderson, Liquid crystal dimers and higher oligomers: between monomers and polymers, Chem. Soc. Rev. 36 (2007) 2096–2124, https://doi.org/10.1039/B714102E.
[8] P.A. Henderson, C.T. Imrie, Methylene-linked liquid crystal dimers and the twist-bend nematic phase, Liq. Cryst. 38 (11–12) (2011) 1407–1414, https://doi.org/10.1080/02678292.2011.624368.
[9] A. Varanytsia, L.-C. Chien, Giant flexoelectro-optic effect with liquid crystal dimer cb7cb, Sci. Rep. 7 (1) (2017) 41333, https://doi.org/10.1038/srep41333.
[10] N. Trbojevic, D.J. Read, M. Nagaraj, Dielectric properties of liquid crystalline dimer mixtures exhibiting the nematic and twist-bend nematic phases, Phys. Rev. E 96 (2017) 052703, https://doi.org/10.1103/PhysRevE.96.052703.
[11] C.T. Imrie, R. Walker, J.M.D. Storey, E. Gorecka, D. Pociecha, Liquid crystal dimers and smectic phases from the intercalated to the twist-bend, Crystals 12 (9) (2022), https://doi.org/10.3390/cryst12091245, https://www.mdpi.com/2073-4352/12/9/1245.
[12] V.P. Panov, J.K. Vij, G.H. Mehl, Twist-bend nematic phase in cyanobiphenyls and difluoroterphenyls bimesogens, Liq. Cryst. 44 (1) (2017) 147–159, https://doi.org/10.1080/02678292.2016.1254289, https://www.tandfonline.com/doi/pdf/10.1080/02678292.2016.1254289.
[13] D. Pociecha, N. Vaupotič, M. Majewska, E. Cruickshank, R. Walker, J.M.D. Storey, C.T. Imrie, C. Wang, E. Gorecka, Photonic bandgap in achiral liquid crystals—a twist on a twist, Adv. Mater. 33 (39) (2021) 2103288, https://doi.org/10.1002/adma.202103288, https://onlinelibrary.wiley.com/doi/pdf/10.1002/adma.202103288, https://onlinelibrary.wiley.com/doi/abs/10.1002/adma.202103288.
[14] C.T. Imrie, P.A. Henderson, G.-Y. Yeap, Liquid crystal oligomers: going beyond dimers, Liq. Cryst. 36 (6–7) (2009) 755–777, https://doi.org/10.1080/02678290903157455.
[15] H. Sasaki, Y. Takanishi, J. Yamamoto, A. Yoshizawa, Achiral flexible liquid crystal trimers exhibiting chiral conglomerates, Soft Matter 12 (2016) 3331–3339, https://doi.org/10.1039/C5SM02969D.
[16] C.T. Imrie, G.R. Luckhurst, Liquid crystal trimers. The synthesis and characterisation of the 4,4′-bis[ω-(4-cyanobiphenyl-4′-yloxy)alkoxy]biphenyls, J. Mater. Chem. 8 (1998) 1339–1343, https://doi.org/10.1039/A801128A.
[17] P.A. Henderson, C.T. Imrie, Non-symmetric liquid crystal trimers, Liq. Cryst. 32 (6) (2005) 673–682, https://doi.org/10.1080/02678290500116235.
[18] T. Donaldson, P.A. Henderson, M.F. Achard, C.T. Imrie, Non-symmetric chiral liquid crystal trimers, Liq. Cryst. 38 (10) (2011) 1331–1339, https://doi.org/10.1080/02678292.2011.613265.
[19] C.T. Imrie, P.A. Henderson, Liquid crystal dimers and oligomers, Curr. Opin. Colloid Interface Sci. 7 (5) (2002) 298–311, https://doi.org/10.1016/S1359-0294(02)00092-4.
[20] G.-Y. Yeap, T.-C. Hng, W.A.K. Mahmood, E. Gorecka, D. Takeuchi, K. Osakada, Novel nonsymmetric trimeric liquid crystals exhibiting glassy nematic state at low temperatures, Mol. Cryst. Liq. Cryst. 487 (1) (2008) 135–152, https://doi.org/10.1080/15421400802198599.
[21] A. Yoshizawa, Unconventional liquid crystal oligomers with a hierarchical structure, J. Mater. Chem. 18 (2008) 2877–2889, https://doi.org/10.1039/B802712A.
[22] S. Malkondu, A. Kocak, Novel liquid crystal trimers with a wide mesophase range, J. Mol. Liq. 188 (2013) 167–172, https://doi.org/10.1016/j.molliq.2013.10.007.
[23] Y.-H. Ooi, G.-Y. Yeap, D. Takeuchi, Synthesis, mesomorphic properties and structural studies on 1, 3,5-trisubstituted benzene-based star-shaped derivatives containing Schiff base ester as the peripheral arm, J. Mol. Struct. 1051 (2013) 361–375, https://doi.org/10.1016/j.molstruc.2013.08.015.
[24] M. Srinatha, S. Poppe, G. Shanker, M. Alaasar, C. Tschierske, 2,3,4-trihydroxy benzonitrile-based liquid crystals: fiber forming room temperature nematic phases, J. Mol. Liq. 317 (2020) 114244, https://doi.org/10.1016/j.molliq.2020.114244.
[25] G. Shanker, M.K. Srinatha, H. Ocak, Effect of polar group on the 2, 3,4-trihydroxy benzonitrile based liquid crystals trimers, Liq. Cryst. 50 (2) (2022) 195–202, https://doi.org/10.1080/02678292.2022.2110955.
[26] W. Haase, H. Pranoto, F.J. Bormuth, Dielectric properties of some side chain liquid crystalline polymers, Ber. Bunsenges. Phys. Chem. 89 (11) (1985) 1229–1234, https://doi.org/10.1002/bbpc.19850891122.
[27] G. Attard, The determination of the order parameters and director alignment in the nematic phase of a liquid crystalline side-chain polymer by the resolution of dielectric loss spectra, Mol. Phys. 58 (6) (1986) 1087–1100, https://doi.org/10.1080/00268978600101821.
[28] K. Araki, G.S. Attard, A. Kozak, G. Williams, G.W. Gray, D. Lacey, G. Nestor, Molecular dynamics of a siloxane liquid-crystalline polymer as studied by dielectric relaxation spectroscopy, J. Chem. Soc. Faraday Trans. 2 (84) (1988) 1067–1081, https://doi.org/10.1039/F29888401067.
[29] M. Grell, D.D.C. Bradley, M. Inbasekaran, E.P. Woo, A glass-forming conjugated main-chain liquid crystal polymer for polarized electroluminescence applications, Adv. Mater. 9 (10) (1997) 798–802, https://doi.org/10.1002/adma.19970091006.
[30] A. Schönhals, U. Geßner, J. Rübner, Influence of lateral substituents in the mesogens on the properties of liquid-crystalline side group copolymethacrylates: dielectric relaxation spectroscopy on homopolymers, Macromol. Chem. Phys. 196 (5) (1995) 1671–1685, https://doi.org/10.1002/macp.1995.021960523.
[31] C. Schick, D. Sukhorukov, A. Schönhals, Comparison of the molecular dynamics of a liquid crystalline side group polymer revealed from temperature modulated dsc and dielectric experiments in the glass transition region, Macromol. Chem. Phys. 202 (8) (2001) 1398–1404, https://doi.org/10.1002/1521-3935(20010501)202:8<1398::AID-MACP1398>3.0.CO;2-C.
[32] F.K.A. Schönhals, Broadband Dielectric Spectroscopy, 1st edition, Springer-Verlag Berlin Heidelberg, 2003.
[33] A. Drozd-Rzoska, S.J. Rzoska, M. Paluch, S. Pawlus, J. Zioło, P.G. Santangelo, C.M. Roland, K. Czupryński, R. Dabrowski, Mode coupling behavior in glass-forming liquid crystalline isopentylcyanobiphenyl, Phys. Rev. E 71 (2005) 011508, https://doi.org/10.1103/PhysRevE.71.011508, https://link.aps.org/doi/10.1103/PhysRevE.71.011508.
[34] A. Drozd-Rzoska, Heterogeneity-related dynamics in isotropic *n*-pentylcyanobiphenyl, Phys. Rev. E 73 (2006) 022501, https://doi.org/10.1103/PhysRevE.73.022501, https://link.aps.org/doi/10.1103/PhysRevE.73.022501.
[35] A. Drozd-Rzoska, S.J. Rzoska, Anomalous decoupling of the dc conductivity and the structural relaxation time in the isotropic phase of a rod-like liquid crystalline compound, in: S. Rzoska, A. Drozd-Rzoska, V. Mazur (Eds.), Metastable Systems Under Pressure, Springer, Netherlands, Dordrecht, 2010, pp. 141–149.
[36] A. Drozd-Rzoska, Glassy dynamics of liquid crystalline 4'-n-pentyl-4-cyanobiphenyl in the isotropic and supercooled nematic phases, J. Chem. Phys. 130 (23) (2009) 234910, https://doi.org/10.1063/1.3153349.
[37] A. Drozd-Rzoska, S. Starzonek, S.J. Rzoska, S. Kralj, Nanoparticle-controlled glassy dynamics in nematogen-based nanocolloids, Phys. Rev. E 99 (2019) 052703, https://doi.org/10.1103/PhysRevE.99.052703, https://link.aps.org/doi/10.1103/PhysRevE.99.052703.
[38] A.R. Brás, M. Dionísio, H. Huth, C. Schick, A. Schönhals, Origin of glassy dynamics in a liquid crystal studied by broadband dielectric and specific heat spectroscopy, Phys. Rev. E 75 (2007) 061708, https://doi.org/10.1103/PhysRevE.75.061708.
[39] J.C. Dyre, Colloquium: the glass transition and elastic models of glass-forming liquids, Rev. Mod. Phys. 78 (2006) 953–972, https://doi.org/10.1103/RevModPhys.78.953, https://link.aps.org/doi/10.1103/RevModPhys.78.953.
[40] G.P. Johari, M. Goldstein, Viscous liquids and the glass transition. II. Secondary relaxations in glasses of rigid molecules, J. Chem. Phys. 53 (6) (1970) 2372–2388, https://doi.org/10.1063/1.1674335.
[41] A. Kudlik, C. Tschirwitz, T. Blochowicz, S. Benkhof, E. Rössler, Slow secondary relaxation in simple glass formers, J. Non-Cryst. Solids 235–237 (1998) 406–411, https://doi.org/10.1016/S0022-3093(98)00510-9.
[42] C.A. Angell, K.L. Ngai, G.B. McKenna, P.F. McMillan, S.W. Martin, Relaxation in glassforming liquids and amorphous solids, J. Appl. Phys. 88 (6) (2000) 3113–3157, https://doi.org/10.1063/1.1286035.
[43] P.G. Debenedetti, F.H. Stillinger, Supercooled liquids and the glass transition, Nature 410 (6825) (2001) 259–267, https://doi.org/10.1038/35065704.
[44] C. Angell, Relaxation in liquids, polymers and plastic crystals - strong/fragile patterns and problems, J. Non-Cryst. Solids 131–133 (1991) 13–31, https://doi.org/10.1016/0022-3093(91)90266-9.
[45] C.A. Angell, Formation of glasses from liquids and biopolymers, Science 267 (5206) (1995) 1924–1935, https://doi.org/10.1126/science.267.5206.1924.
[46] F. Stickel, E.W. Fischer, R. Richert, Dynamics of glass-forming liquids. II. Detailed comparison of dielectric relaxation, dc-conductivity, and viscosity data, J. Chem. Phys. 104 (5) (1996) 2043–2055, https://doi.org/10.1063/1.470961.
[47] V.N. Novikov, A.P. Sokolov, Universality of the dynamic crossover in glass-forming liquids: a "magic" relaxation time, Phys. Rev. E 67 (2003) 031507, https://doi.org/10.1103/PhysRevE.67.031507, https://link.aps.org/doi/10.1103/PhysRevE.67.031507.
[48] A. Kudlik, C. Tschirwitz, S. Benkhof, T. Blochowicz, E. Rössler, Slow secondary relaxation process in supercooled liquids, Europhys. Lett. 40 (6) (1997) 649–654, https://doi.org/10.1209/epl/i1997-00518-y.
[49] K.L. Ngai, P. Lunkenheimer, C. León, U. Schneider, R. Brand, A. Loidl, Nature and properties of the Johari–Goldstein β-relaxation in the equilibrium liquid state of a class of glass-formers, J. Chem. Phys. 115 (3) (2001) 1405–1413, https://doi.org/10.1063/1.1381054.
[50] A. Schönhals, Evidence for a universal crossover behaviour of the dynamic glass transition, Europhys. Lett. 56 (6) (2001) 815–821, https://doi.org/10.1209/epl/i2001-00115-8.
[51] M. Goldstein, Viscous liquids and the glass transition: a potential energy barrier picture, J. Chem. Phys. 51 (9) (1969) 3728–3739, https://doi.org/10.1063/1.1672587.
[52] J. Colmenero, Are polymers standard glass-forming systems? The role of intramolecular barriers on the glass-transition phenomena of glass-forming polymers, J. Phys. Condens. Matter 27 (10) (2015) 103101, https://doi.org/10.1088/0953-8984/27/10/103101.
[53] D.L. Baker, M. Reynolds, R. Masurel, P.D. Olmsted, J. Mattsson, Cooperative intramolecular dynamics control the chain-length-dependent glass transition in polymers, Phys. Rev. X 12 (2022) 021047, https://doi.org/10.1103/PhysRevX.12.021047, https://link.aps.org/doi/10.1103/PhysRevX.12.021047.
[54] J. Mattsson, R. Bergman, P. Jacobsson, L. Börjesson, Chain-length-dependent relaxation scenarios in an oligomeric glass-forming system: from merged to well-separated α and β loss peaks, Phys. Rev. Lett. 90 (2003) 075702, https://doi.org/10.1103/PhysRevLett.90.075702, https://link.aps.org/doi/10.1103/PhysRevLett.90.075702.

[55] R. Casalini, C.M. Roland, S. Capaccioli, Effect of chain length on fragility and thermodynamic scaling of the local segmental dynamics in poly(methylmethacrylate), J. Chem. Phys. 126 (18) (2007) 184903, https://doi.org/10.1063/1.2728898.

[56] C.M. Roland, Relaxation phenomena in vitrifying polymers and molecular liquids, Macromolecules 43 (19) (2010) 7875–7890, https://doi.org/10.1021/ma101649u.

[57] P.L. Nordio, G. Rigatti, U. Segre, Dielectric relaxation theory in nematic liquids, Mol. Phys. 25 (1) (1973) 129–136, https://doi.org/10.1080/00268977300100141.

[58] M.R. de la Fuente, D. Dunmur, Dielectric properties of liquid crystals, in: J. Goodby, P. Collings, T. Kato, C. Tschierske, H. Gleeson, P. Raynes, V. Vill (Eds.), Handbook of Liquid Crystals, vol. 2, 2nd edition, John Wiley & Sons, Ltd, 2014, Ch. 4.

[59] W. Maier, G. Meier, Eine einfache theorie der dielektrischen eigenschaften homogen orientierter kristallinflüssiger phasen des nematischen typs, Z. Naturforsch. A 16 (3) (1961) 262–267, https://doi.org/10.1515/zna-1961-0309.

[60] G. Meier, A. Saupe, Dielectric relaxation in nematic liquid crystals, Mol. Cryst. 1 (4) (1966) 515–525, https://doi.org/10.1080/15421406608083290.

[61] R. Zentel, G.R. Strobl, H. Ringsdorf, Dielectric relaxation of liquid crystalline polyacrylates and polymethacrylates, Macromolecules 18 (5) (1985) 960–965, https://doi.org/10.1021/ma00147a026.

[62] J.F. Mano, Cooperative character of the relaxation processes in a side-chain liquid crystalline polymer, J. Macromol. Sci., Part B 42 (6) (2003) 1169–1182, https://doi.org/10.1081/MB-120024812.

[63] A. Schönhals, D. Wolff, J. Springer, Dependence of the molecular dynamics of comblike polyacrylates and polymethacrylates on the mesophase structure studied by dielectric spectroscopy, in: P.F. Gobin, J. Tatibouet (Eds.), 3rd International Conference on Intelligent Materials and 3rd European Conference on Smart Structures and Materials, in: International Society for Optics and Photonics, vol. 2779, SPIE, 1996, pp. 424–429.

[64] A. Schönhals, D. Wolff, J. Springer, Temperature dependence of the relaxation rates of α and δ relaxation in liquid-crystalline side-group polymethacrylates, Macromolecules 31 (25) (1998) 9019–9025, https://doi.org/10.1021/ma9715381.

[65] A. Schönhals Hans-eckartcarius, Dielectric properties of thermotropic polymer liquid crystals, Int. J. Polym. Mater. Polym. Biomater. 45 (3–4) (2000) 239–276, https://doi.org/10.1080/00914030008035046.

[66] S. Zhukov, B. Stühn, T. Borisova, E. Barmatov, M. Barmatova, V. Shibaev, F. Kremer, P. Pissis, Dielectric and ir spectroscopy of the macromolecular reaction of anhydridization in a functionalized side-chain liquid crystalline copolymer containing acrylic acid groups, Macromolecules 34 (11) (2001) 3615–3625, https://doi.org/10.1021/ma0018401.

[67] G. Turky, D. Wolff, A. Schönhals, Confinement effects on the molecular dynamics of liquid-crystalline polymethacrylates—a broadband dielectric spectroscopy study, Macromol. Chem. Phys. 213 (22) (2012) 2420–2431, https://doi.org/10.1002/macp.201200361.

[68] T. Raistrick, M. Reynolds, H.F. Gleeson, J. Mattsson, Influence of liquid crystallinity and mechanical deformation on the molecular relaxations of an auxetic liquid crystal elastomer, Molecules 26 (23) (2021), https://doi.org/10.3390/molecules26237313, https://www.mdpi.com/1420-3049/26/23/7313.

[69] U. Geßner, J. Rübner, J. Springer, The influence of lateral substituents in the mesogens of liquid crystalline side group copolymethacrylates on the phase behaviour, J. Prakt. Chem. 337 (1) (1995) 582–588, https://doi.org/10.1002/prac.199533701122.

[70] U. Gedde, F. Liu, A. Hult, F. Sahlén, R. Boyd, Dielectric relaxation of liquid crystalline side-chain poly(vinyl ether)s, Polymer 35 (10) (1994) 2056–2062, https://doi.org/10.1016/0032-3861(94)90228-3.

[71] A. Schönhals, D. Wolff, J. Springer, Influence of the mesophase structure on the β relaxation in comb-like polymethacrylates, Macromolecules 28 (18) (1995) 6254–6257, https://doi.org/10.1021/ma00122a036.

[72] K.L. Ngai, A. Schönhals, Interpretation of the observed influence of mesophase structures on the β relaxation in side chain liquid crystal polymers, J. Polym. Sci., Part B, Polym. Phys. 36 (11) (1998) 1927–1934, https://doi.org/10.1002/(SICI)1099-0488(199808)36:11<1927::AID-POLB14>3.0.CO;2-9.

[73] Z. Jiang, C.T. Imrie, J.M. Hutchinson, An introduction to temperature modulated differential scanning calorimetry (tmdsc): a relatively non-mathematical approach, Thermochim. Acta 387 (1) (2002) 75–93, https://doi.org/10.1016/S0040-6031(01)00829-2, https://www.sciencedirect.com/science/article/pii/S0040603101008292.

[74] C.T. Moynihan, A.J. Easteal, M.A. De Bolt, J. Tucker, Dependence of the fictive temperature of glass on cooling rate, J. Am. Ceram. Soc. 59 (1–2) (1976) 12–16, https://doi.org/10.1111/j.1151-2916.1976.tb09376.x, https://ceramics.onlinelibrary.wiley.com/doi/pdf/10.1111/j.1151-2916.1976.tb09376.x, https://ceramics.onlinelibrary.wiley.com/doi/abs/10.1111/j.1151-2916.1976.tb09376.x.

[75] J.C. Jones, Handbook of Optoelectronics: Volume 2, CRC Press, 2017, Ch. 6.

[76] S. Havriliak, S. Negami, A complex plane representation of dielectric and mechanical relaxation processes in some polymers, Polymer 8 (1967) 161–210, https://doi.org/10.1016/0032-3861(67)90021-3.

[77] K.S. Cole, R.H. Cole, Dispersion and absorption in dielectrics I. Alternating current characteristics, J. Chem. Phys. 9 (4) (1941) 341–351, https://doi.org/10.1063/1.1750906.

[78] D.J. Plazek, 1995 Bingham medal address: oh, thermorheological simplicity, wherefore art thou?, J. Rheol. 40 (6) (1996) 987–1014, https://doi.org/10.1122/1.550776.

[79] R.H. Colby, J.R. Gillmor, G. Galli, M. Laus, C.K. Ober, E. Hall, Linear viscoelasticity of side chain liquid crystal polymer, Liq. Cryst. 13 (2) (1993) 233–245, https://doi.org/10.1080/02678299308026297.

[80] S.F. Rubin, R.M. Kannan, J.A. Kornfield, C. Boeffel, Effect of mesophase order and molecular weight on the dynamics of nematic and smectic side-group liquid-crystalline polymers, Macromolecules 28 (10) (1995) 3521–3530, https://doi.org/10.1021/ma00114a005.

[81] K.M. Lee, C.D. Han, Effect of flexible spacer length on the rheology of side-chain liquid-crystalline polymers, Macromolecules 36 (23) (2003) 8796–8810, https://doi.org/10.1021/ma030303o.

[82] M.L. Auad, M.D. Kempe, J.A. Kornfield, S. Rendon, W.R. Burghardt, K. Yoon, Effect of mesophase order on the dynamics of side group liquid crystalline polymers, Macromolecules 38 (16) (2005) 6946–6953, https://doi.org/10.1021/ma050551f.

[83] J. Li, S.-T. Wu, Two-coefficient Cauchy model for low birefringence liquid crystals, J. Appl. Phys. 96 (1) (2004) 170–174, https://doi.org/10.1063/1.1738526.

[84] R. Dabrowski, P. Kula, J. Herman, High birefringence liquid crystals, Crystals 3 (3) (2013) 443–482, https://doi.org/10.3390/cryst3030443.

[85] L.-M. Wang, C.A. Angell, R. Richert, Fragility and thermodynamics in nonpolymeric glass-forming liquids, J. Chem. Phys. 125 (7) (2006) 074505, https://doi.org/10.1063/1.2244551.

[86] K. Ngai, C. Roland, Chemical structure and intermolecular cooperativity: dielectric relaxation results, Macromolecules 26 (25) (1993) 6824–6830.

[87] A. Hensel, C. Schick, Relation between freezing-in due to linear cooling and the dynamic glass transition temperature by temperature-modulated dsc, J. Non-Cryst. Solids 235–237 (1998) 510–516, https://doi.org/10.1016/S0022-3093(98)00607-3, https://www.sciencedirect.com/science/article/pii/S0022309398006073.

[88] M.A. Ratner, P. Johansson, D.F. Shriver, Polymer electrolytes: ionic transport mechanisms and relaxation coupling, Mater. Res. Soc. Bull. 25 (3) (2000) 31–37, https://doi.org/10.1557/mrs2000.16.

[89] Y. Wang, F. Fan, A.L. Agapov, X. Yu, K. Hong, J. Mays, A.P. Sokolov, Design of superionic polymers—new insights from walden plot analysis, Solid State Ion. 262 (2014) 782–784, https://doi.org/10.1016/j.ssi.2013.09.026, Solid State Ionics 19, Proceedings of the 19th International Conference on Solid State Ionics, https://www.sciencedirect.com/science/article/pii/S0167273813004359.

[90] A.L. Agapov, A.P. Sokolov, Decoupling ionic conductivity from structural relaxation: a way to solid polymer electrolytes?, Macromolecules 44 (11) (2011) 4410–4414, https://doi.org/10.1021/ma2001096.

[91] V. Bocharova, A.P. Sokolov, Perspectives for polymer electrolytes: a view from fundamentals of ionic conductivity, Macromolecules 53 (11) (2020) 4141–4157, https://doi.org/10.1021/acs.macromol.9b02742.

[92] K. Kishimoto, T. Suzawa, T. Yokota, T. Mukai, H. Ohno, T. Kato, Nano-segregated polymeric film exhibiting high ionic conductivities, J. Am. Chem. Soc. 127 (44) (2005) 15618–15623, https://doi.org/10.1021/ja0549594, pMID: 16262428.

[93] T. Kato, M. Yoshio, T. Ichikawa, B. Soberats, H. Ohno, M. Funahashi, Transport of ions and electrons in nanostructured liquid crystals, Nat. Rev. Mater. 2 (4) (2017) 17001, https://doi.org/10.1038/natrevmats.2017.1.

[94] P.W. Majewski, M. Gopinadhan, W.-S. Jang, J.L. Lutkenhaus, C.O. Osuji, Anisotropic ionic conductivity in block copolymer membranes by magnetic field alignment, J. Am. Chem. Soc. 132 (49) (2010) 17516–17522, https://doi.org/10.1021/ja107309p, pMID: 21090713.

[95] Z. Stoeva, Z. Lu, M.D. Ingram, C.T. Imrie, A new polymer electrolyte based on a discotic liquid crystal triblock copolymer, Electrochim. Acta 93 (2013) 279–286, https://doi.org/10.1016/j.electacta.2013.01.060.

[96] S. Wang, X. Liu, A. Wang, Z. Wang, J. Chen, Q. Zeng, X. Jiang, H. Zhou, L. Zhang, High-performance all-solid-state polymer electrolyte with controllable conductivity pathway formed by self-assembly of reactive discogen and immobilized via a facile photopolymerization for a lithium-ion battery, ACS Appl. Mater. Interfaces 10 (30) (2018) 25273–25284, https://doi.org/10.1021/acsami.8b04672, pMID: 29975039.

[97] C.T. Imrie, M.D. Ingram, G.S. McHattie, Ion transport in glassy side-group liquid crystalline polymer electrolytes, Adv. Mater. 11 (10) (1999) 832–834, https://doi.org/10.1002/(SICI)1521-4095(199907)11:10<832::AID-ADMA832>3.0.CO;2-Z.

[98] C.A. Angell, C.T. Imrie, M.D. Ingram, From simple electrolyte solutions through polymer electrolytes to superionic rubbers: some fundamental considerations, Polym. Int. 47 (1) (1998) 9–15, https://doi.org/10.1002/(SICI)1097-0126(199809)47:1<9::AID-PI69>3.0.CO;2-1.

[99] F. Stickel, E.W. Fischer, R. Richert, Dynamics of glass-forming liquids. I. Temperature-derivative analysis of dielectric relaxation data, J. Chem. Phys. 102 (15) (1995) 6251–6257, https://doi.org/10.1063/1.469071.

[100] W. Haase, F.J. Bormuth, M. Pfciffer, E. Jakob, Molecular motions in liquid crystal side-chain polymers, Ber. Bunsenges. Phys. Chem. 95 (9) (1991) 1050–1054, https://doi.org/10.1002/bbpc.19910950920.

[101] A. Schönhals, R. Ruhmann, T. Thiele, D. Prescher, Photonic and Optoelectronic Polymers, American Chemical Society, 1997, pp. 280–296, Ch. 19.

[102] Y.S. Lipatov, V.V. Tsukruk, V.V. Shilov, Recent successes in structural studies of thermotropic liquid crystalline polymers, J. Macromol. Sci., Part C 24 (2) (1984) 173–238, https://doi.org/10.1080/07366578408079447.

[103] S. Koltzenburg, D. Wolff, J. Springer, O. Nuyken, Novel study on the liquid crystalline behavior of poly(methacrylate)s with biphenyl side groups, J. Polym. Sci., Part A, Polym. Chem. 36 (15) (1998) 2669–2679, https://doi.org/10.1002/(SICI)1099-0518(19981115)36:15<2669::AID-POLA1>3.0.CO;2-4.

[104] G. Rodekirch, J. Rübner, V. Zschuppe, D. Wolff, J. Springer, New side-group liquid-crystalline polymethacrylates, Makromol. Chem. 194 (4) (1993) 1125–1135, https://doi.org/10.1002/macp.1993.021940408.

[105] A. Schönhals, H. Goering, C. Schick, B. Frick, R. Zorn, Polymers in nanoconfinement: what can be learned from relaxation and scattering experiments?, J. Non-Cryst. Solids 351 (33) (2005) 2668–2677, https://doi.org/10.1016/j.jnoncrysol.2005.03.062, Proceedings of 3rd International Conference on Broadband Dielectric Spectroscopy and its Applications.

[106] A. Schönhals, H. Goering, C. Schick, B. Frick, M. Mayorova, R. Zorn, Segmental dynamics of poly(methyl phenyl siloxane) confined to nanoporous glasses, Eur. Phys. J. Spec. Top. 141 (1) (2007) 255–259, https://doi.org/10.1140/epjst/e2007-00049-3.

[107] M. Stocchero, A. Ferrarini, G.J. Moro, D.A. Dunmur, G.R. Luckhurst, Molecular theory of dielectric relaxation in nematic dimers, J. Chem. Phys. 121 (16) (2004) 8079–8097, https://doi.org/10.1063/1.1794071.

[108] N. Sebastián, B. Robles-Hernández, S. Diez-Berart, J. Salud, G.R. Luckhurst, D.A. Dunmur, D.O. López, M.R. de la Fuente, Distinctive dielectric properties of nematic liquid crystal dimers, Liq. Cryst. 44 (1) (2017) 177–190, https://doi.org/10.1080/02678292.2016.1218963.

[109] D.O. López, N. Sebastian, M.R. de la Fuente, J.C. Martínez-García, J. Salud, M.A. Pérez-Jubindo, S. Diez-Berart, D.A. Dunmur, G.R. Luckhurst, Disentangling molecular motions involved in the glass transition of a twist-bend nematic liquid crystal through dielectric studies, J. Chem. Phys. 137 (3) (2012) 034502, https://doi.org/10.1063/1.4733561.

[110] D.O. López, J. Salud, M.R. de la Fuente, N. Sebastián, S. Diez-Berart, Cooperative behavior of molecular motions giving rise to two glass transitions in the same supercooled mesophase of a smectogenic liquid crystal dimer, Phys. Rev. E 97 (2018) 012704, https://doi.org/10.1103/PhysRevE.97.012704.

[111] D.A. Dunmur, G.R. Luckhurst, M.R. de la Fuente, S. Diez, M.A. Peréz Jubindo, Dielectric relaxation in liquid crystalline dimers, J. Chem. Phys. 115 (18) (2001) 8681–8691, https://doi.org/10.1063/1.1409365.